Article:
Halliday, David orcid.org/0000-0001-9957-0983, Brittain, John-Stuart, Stevenson, Carl W et al. (1 more author) (2018) Adaptive spectral tracking for coherence estimation:the z-tracker. Journal of Neural Engineering. 026004. ISSN 1741-2552

https://doi.org/10.1088/1741-2552/aaa3b4

Adaptive Spectral Tracking for Coherence Estimation: The z-tracker.

David M. Halliday[1], John-Stuart Brittain[2*], Carl W. Stevenson[3], and Rob Mason[4]

[1]Department of Electronic Engineering, University of York, YORK, Y010 5DD, UK
[2]MRC Brain Network Dynamics Unit, University of Oxford, Oxford, OX1 3TH, UK
[3]School of Biosciences, University of Nottingham, Loughborough LE12 5RD, UK
[4]School of Life Sciences, University of Nottingham, Nottingham, NG7 2UH, UK

E-mail: `david.halliday@york.ac.uk`

*Current address: School of Psychology, University of Birmingham, Birmingham, B15 2TT, UK

Revised 20 Dec 2017.

Abstract.
Objective. A major challenge in non-stationary signal analysis is reliable estimation of correlation. Neurophysiological recordings can be many minutes in duration with data that exhibits correlation which changes over different time scales. Local smoothing can be used to estimate time-dependency, however, an effective framework needs to adjust levels of smoothing in response to changes in correlation. *Approach.* Here we present a novel data-adaptive algorithm, the z-tracker, for estimating local correlation in segmented data. The algorithm constructs single segment coherence estimates using multi-taper windows. These are subject to adaptive Kalman filtering/smoothing in the z-domain to construct a local coherence estimate for each segment. The error residual for each segment determines the levels of process noise, allowing the filter to adapt rapidly to sudden changes in correlation while applying greater smoothing to data where the correlation is consistent across segments. The method is compared to wavelet coherence, calculated using orthogonal Morse wavelets. *Main Results.* The performance of the z-tracker is quantified against Morse wavelet coherence using a Mean Square Deviation (MSD) metric. The z-tracker has significantly lower MSD than the wavelet estimate for time-varying coherence over long time scales ($\sim 10 - 20$ sec), whereas the wavelet has lower MSD for coherence varying over short time scales ($\sim 1 - 2$ sec). The z-tracker also has a lower MSD for slowly varying coherence with occasional step changes. The method is applied to detect changes in coherence in paired LFP recordings from rat prefrontal cortex and amygdala in response to a pharmacological challenge. *Significance.* The z-tracker provides an effective and efficient method to estimate time varying correlation in multivariate data, leading to better characterisation of neurophysiology signals where correlation is subject to slow modulation over time. A number of suggestions are included for future refinements.

Keywords: Non-stationary, time-frequency, Morse wavelet, Kalman filter, spectra, coherence.

Submitted to: *J. Neural Eng.*

1. Introduction

Large data sets are routinely collected in neuroscience. These can be subject to a wide range of statistical analysis to address basic questions relating to underlying features in the data or to test specific hypotheses. One question that is commonly asked in the case of multivariate random processes - is there any correlation between the signals? Here we present a new technique that can be used to undertake an exploratory analysis of time-varying correlation. The method relies on segmentation of the data into short non-overlapping segments, an approach often used in multi-taper (MT) and other spectral analysis methods. It provides a rapid, quantitative characterisation of the correlation structure on a segment by segment basis. This is achieved using smoothing within each segment through application of multi-taper spectral estimates, combined with local smoothing across segments by using Kalman filtering/smoothing. The approach can readily be undertaken as an addition to a bivariate spectral analysis, here we demonstrate its application to neurophysiological data.

The concept of time-frequency analysis is well established [20, 23]. Two broad classes of methods can be identified, spectrograms and wavelets. Spectrograms involve segmentation of data into short segments using a sliding data window to extract local features [2, 51, 52], these are closely related to classical spectral estimation based on overlapping data windows [50]. Wavelet methods are increasingly used [1, 8, 48, 52]. Much of the wavelet work uses continuous wavelets, a popular choice is the complex Morlet wavelet [48] however analytic wavelets can also be used to estimate coherence and phase for bivariate data [29, 30, 36]. The Morse family of analytic wavelets has theoretical and practical advantages over Morlet wavelets [28]. Statistical properties of coherence estimates using temporally smoothed Morlet wavelets [17] and analytic Morse wavelets [18] have been derived, allowing rigorous hypothesis testing on wavelet coherence estimates. In this study we use wavelet coherence estimates as the benchmark against which to compare the performance of our approach, in particular coherence based on analytic Morse wavelets [8, 17].

Our method combines multi-taper analysis [38, 46] with Kalman filtering [27] to allow rapid screening of long data sets for correlated activity. Multi-taper methods are well established for spectral and coherence analysis of neural signals [16]. Novelty is in the combined application of multi-taper spectral analysis with a Kalman filtering/smoothing algorithm [25] which adjusts the level of smoothing in a data adaptive manner based on the Kalman filter residual error term. Higher levels of local smoothing are applied to data with low residual errors. In contrast large residuals, resulting from a sudden change in correlation structure, have a larger Kalman gain allowing the algorithm to adapt to sudden changes in the correlation structure. The algorithm operates in the z domain, thus we refer to the approach as the z-tracker.

The z-tracker is a non-parametric approach, using Kalman filtering applied to single segment coherence estimates derived from Fourier transforms. In [3] a non-parametric approach is described which uses a Bayesian framework to apply temporal smoothing to a small number of pre-specified frequencies using fixed interval smoothing [42]. The z-tracker described here uses the same approach to smoothing. Parametric approaches have been considered to estimate time varying coherence. In [34] adaptive estimation of multivariate auto-regressive model parameters was used to construct time-varying coherence estimates. In [33] this was extended to use Kalman filter estimates of a multivariate state-space signal model to study time dependency in local field potential interactions.

The z-tracker is applied to surrogate data with a known correlation structure and the performance is compared with Morse wavelet coherence estimates, and quantified empirically using a mean square deviation (MSD) metric to assess accuracy of estimates, and comparison of the Kalman filter mean square error (MSE) with the variance of the Morse wavelet estimates, based on their known degrees of freedom [17]. Three scenarios are considered for the surrogate data: 1) Slowly varying coherence, time scale $\sim 10-20$ sec, 2) Rapidly varying coherence, time scale $\sim 1-2$ sec, and 3) Slowly varying coherence with occasional step changes. The motivation for these three scenarios is the wide range of time scales over which interactions in brain activity can alter [44]. We find that the z-tracker is more accurate, with a lower MSD than the Morse wavelet coherence in scenarios 1 and 3, whereas the Morse wavelet estimate has lower MSD in scenario 2. We further empirically compare the performance on uncorrelated surrogate data and find the performance of the two approaches similar as assessed using the MSD. To illustrate application of the method to experimental data we apply the z-tracker to *in vivo* electrophysiological recordings of local field potentials from anaesthetised rat.

Section 2 describes the z-tracker algorithm, with construction of single segment coherence estimates in section 2.1, adaptive Kalman filtering and smoothing in section 2.2, and the method for obtaining estimates of the variance and bias of single segment z estimates in section 2.3. Section 2.4 briefly describes the wavelet coherence measure used to benchmark the performance of the z-tracker. Section 3.1 describes the generation of surrogate data, sections 3.2 to 3.4 illustrate the three scenarios for changing correlation structure, section 3.5

considers how the Kalman filter error estimate can be used to construct point-wise confidence limits, section 3.6 examines the performance of the z-tracker on uncorrelated surrogate data, and results from analysis of *in vivo* experimental data are presented in section 3.7. Section 3.8 discusses briefly the computational complexity of the z-tracker and wavelet approaches. Conclusions and discussion are in section 4.

2. Methods

The z-tracker is a two stage process. First single segment coherence estimates are constructed using MT estimates [38], second these single segment estimators are subject to Kalman filtering and smoothing [11] which provides local estimates of the coherence while reducing the statistical variability. An empirical approach for setting point-wise confidence limits using the Kalman filter error estimate is described. We briefly introduce the Morse wavelet coherence estimator as the benchmark against which the z-tracker is compared for the simulations described in section 3.

In this study bivariate random processes, (x, y), are assumed to be oscillatory or sigma-oscillatory processes. An example of an oscillatory process, z_t, is $z_t \equiv g_t x_t$, where x_t is a process stationary to second order, and g_t a deterministic real-valued modulating function whose Fourier transform has a maximum at zero frequency. Such processes are also referred to as uniformly modulated processes [40, Ch 6], the spectrum of z_t is uniformly modulated at all frequencies compared to the spectrum of x_t. The coherence between two uniformly modulated processes does not vary over time [49], thus they are not suitable for modelling time-varying coherence. A sigma-oscillatory process is one which can be modelled as a sum of oscillatory processes at each time point. The coherence between an oscillatory process and sigma-oscillatory process or between two sigma-oscillatory processes can vary over time [19]. We use surrogate data with one oscillatory and one sigma-oscillatory process to test the performance of the z-tracker in section 3, the generation of these processes is described in section 3.1.

2.1. Single segment coherence estimators

The data for each process (x, y) is split into L non-overlapping segments of T points. The choice of segment length T is important, and is discussed in the results. In order to construct coherence estimates from single segments a MT approach is used [46]. A standard periodogram method would not work, coherence constructed from a single segment would be identically 1 at all frequencies. The MT method applies a series of orthogonal tapers to single segments [38]. The MT Fourier transform of a single segment, l, $l = 1, \ldots, L$ of length T from process x is

$$d_{x,k}^{T(mt)}(\lambda_j, l) = \sqrt{T} \sum_{t=(l-1)T}^{lT-1} h_{t,k}\, x_t\, e^{-i\lambda_j t}. \quad (1)$$

Here $h_{t,k}$ is the orthogonal taper of order k, where $k = 0, \ldots, K-1$, K is the total number of tapers applied, and the λ_j are the Fourier frequencies, $j = 0, \ldots, T/2$. The orthogonal tapers used in MT spectral estimation are derived from Slepian sequences [38, 46]. The $\sqrt{T}$ multiplier is incorporated as a data window normalisation factor [4] to preserve the scaling on spectral estimates [24]. A similar expression gives $d_{y,k}^{T(mt)}(\lambda_j, l)$. An MT cross-spectral estimate for a single segment is

$$\hat{f}_{yx}^{(mt)}(\lambda_j, l) = \frac{1}{2\pi KT} \sum_{k=0}^{K-1} d_{y,k}^{T(mt)}(\lambda_j, l)\, \overline{d_{x,k}^{T(mt)}(\lambda_j, l)}. \quad (2)$$

The symbol, $\hat{}$, denotes an estimate, the overbar indicates a complex conjugate. Smoothing is incorporated in equation 2 through application of orthogonal tapers to the same segment. A similar approach gives the estimates $\hat{f}_{xx}^{(mt)}(\lambda_j, l)$ and $\hat{f}_{yy}^{(mt)}(\lambda_j, l)$. These estimates can be combined to give a single segment coherence estimate for segment l

$$|\hat{R}_{yx}^{(mt)}(\lambda_j, l)|^2 = \frac{|\hat{f}_{yx}^{(mt)}(\lambda_j, l)|^2}{\hat{f}_{xx}^{(mt)}(\lambda_j, l)\, \hat{f}_{yy}^{(mt)}(\lambda_j, l)}. \quad (3)$$

The number of tapers K is determined from the time $\times$ half-bandwidth product, NW, according to the relationship $K \sim 2NW - 1$ [38]. In the z-tracker analysis NW is fixed at $NW = 1.5$ and $K = 2$, this is the smallest value of K which will give coherence estimates not equal to 1. Although we have constructed coherence estimates from single segments of data, these have poor statistical properties (examined in section 2.3) so further smoothing is required. In the z-tracker framework this additional smoothing uses Kalman filtering and smoothing.

2.2. Kalman filtering and adaptive spectral tracking

The first step is application of the variance stabilising z-transform [5, 7, 43]. This transform disproportionately increases values of coherence closer to 1, the effect of which is to generate an estimate (in the z domain) that has a distribution closer to a normal distribution [47], matching more closely the assumptions for Kalman filtering. Kalman filtering and smoothing are applied to the z-transformed coherence, once filtering/smoothing is complete an inverse transform is applied to convert back to the coherence domain. Since Kalman filtering/smoothing is applied in the z-domain we refer to the approach as the z-tracker. The

z-transform is applied to the magnitude square root of the coherence, called coherency [7], as

$$\hat{z}_{yx}^{(mt)}(\lambda_j, l) = tanh^{-1}|\hat{R}_{yx}^{(mt)}(\lambda_j, l)|. \quad (4)$$

The z-tracker operates in the z-domain, taking as input the real-valued $\hat{z}_{yx}^{(mt)}(\lambda_j, l)$ for each segment. The Kalman filter uses a state model that assumes the coherence is constant between segments. Smoothing is incorporated using fixed interval smoothing over all available segments [42]. Smoothing can overcome the tracking delay associated with estimates based only on Kalman filtering and further reduces the variability of coherence estimates by conditioning the estimate locally on segments before and after the current segment. Smoothing requires access to the complete record, this is normal in electrophysiological signal analysis, but would have implications for real time applications. Section 3 compares filtered and smoothed estimates using simulated data. Full details of the Kalman filtering and smoothing steps are given in Appendix A.

The adaptive algorithm determines an appropriate variance for the process noise, q_l, at each step in the forward pass based on the values of the measurement residual in the Kalman filter. In our case this measurement residual for segment l is $\mathbf{e}_l = (\mathbf{z}_l - \mathbf{x}_l^p)$, see equation A.3. This residual represents the difference between the actual and estimated measurements and can be used as an indicator of the system encountering unexpected data. The approach adopted here is the same as [10], following [25].

The adaptive algorithm compares the residual variance with the residual variance assuming no process noise. [25] proposes using $\|\mathbf{e}_l\|^2$ as an indicator of $E\{\mathbf{e}_l^2\}$. In our case $\mathbf{z}_l$, $\mathbf{x}_l$ and $\mathbf{e}_l$ are vectors over the frequency range of interest. The residual variance with no process noise, $E\{\mathbf{e}_l^2|q \equiv 0\}$, is derived from the Kalman filter equations A.1 and A.2 with the assumption that $\mathbf{w}_l = 0$ [25]. In our case

$$E\{\mathbf{e}_l^2|q \equiv 0\} = P_{l-1} + r_l. \quad (5)$$

From this the instantaneous process noise variance denoted by q_l' can be calculated as the excess of the residual variance over the estimated residual variance with no process noise

$$q_l' = \Theta\left(\frac{\mathbf{e}_l^T \mathbf{e}_l}{N} - (P_{l-1} + r_l)\right). \quad (6)$$

Here $\Theta()$ is the Heaviside function, the superscript T refers to a matrix transpose and N is the number of points in the error vector used to estimate the residual variance.

As pointed out by [25] this single value q_l' is likely to be of limited use, as it is based on only a single residual. To overcome this issue we use additional smoothing based on the same approach as the univariate case [10]. A smoothed version of the process noise for segment l denoted as q_l, is determined according to

$$q_l = \alpha\, q_{l-1} + (1-\alpha) q_l' \quad (7)$$

where the parameter α ($\alpha < 1$) controls the exponential smoothing to generate q_l. This noise process is initialised as $q_1 = 0$. The value of α has to be specified in advance, section 3 compares the performance of the z-tracker for a range of α values using simulated data with known target coherence.

Tracking (equations A.3-A.4) or smoothing (equations A.7-A.8) generates a filtered or smoothed estimate, respectively, in the z-domain. The final coherence estimate for each segment is obtained by applying the bias correction, in the z-domain using the bias correction look up table (described in section 2.3) followed by mapping back to the coherence domain. Bias correction is applied separately at each frequency, λ_j, and each segment, l, as

$$|\hat{R}_{yx}(\lambda_j, l)|^2 = tanh\left(\hat{z}_{yx}(\lambda_j, l) - B\left(\hat{z}_{yx}(\lambda_j, l)\right)\right)^2 \quad (8)$$

where the function $B(\cdot)$ refers to the bias correction defined in section 2.3.

The Kalman filter error term is used to approximate the variance of the filtered/smoothed estimate as

$$var\{\hat{z}_{yx}(\lambda_j, l)\} = P_l. \quad (9)$$

From this 95% point-wise confidence limits in the z-domain can be added to the bias corrected estimate of z as $\pm 1.96\sqrt{P_l}$, these can be mapped to the coherence domain for plotting.

An algorithmic level description of the z-tracker is given in Appendix B.

2.3. Variance and Bias of z-transformed single segment multi-taper coherency estimates

The variance and bias associated with coherence estimates have been widely documented [5, 7, 13, 14, 47], and approximate expressions for these are available [5, 47]. Expressions for the distribution of coherence are given in [7, 14, 21], these use the hypergeometric function with true coherence as an argument. The standard approximations for variance and bias are the result of using simulation studies [15, 21]. The approximation for the variance is $var\left\{\hat{z}_{yx}^{(mt)}(\lambda_j, l)\right\} = \frac{1}{2(K-1)}$, where K is the number of independent terms used in the coherence estimate [5, 47]. This expression has been applied to z-transformed coherence estimates constructed using average periodograms from non-overlapped segments, where K is the number of segments. For large K the approximation $\frac{1}{2K}$ is sometimes used [24]. The bias of z-transformed

coherence estimates is usually approximated as $\frac{1}{2(K-1)}$ [5, 47].

For the estimate in equation 4 with $K = 2$ the above approximations give $var\{\hat{z}\} = 0.5$, and a bias of 0.5. However, these approximations are only valid when the true coherence is within the range 0.4 to 0.95 and a minimum of $K = 10$ segments (or orthogonal tapers) have been used in constructing the coherence estimate [21]. Further results are given in [13] for K in the range 32 to 64 which highlight that the variance is not constant over all values of coherence.

In the Kalman filter, the noise variance for each segment, r_l, is taken as the variance of the z-transformed single segment MT estimate in equation 4. We adopt the approach of [21] and undertake a simulation study to evaluate the variance of and bias in equation 4. Results are shown in figure 1 using 101 target z values linearly spaced from 0 to 3 (0 to 0.99 coherence) with 10000 repetitions at each value. Bivariate data was generated as described in section 3.1 using a single segment of $T = 1024$ points. Coherence estimates were constructed using equation 3, with $NW = 1.5$, $K = 2$. The variance was taken as the variance over all frequencies and repetitions at each target z, the bias as the difference between the mean over all frequencies and repetitions and the target value of z.

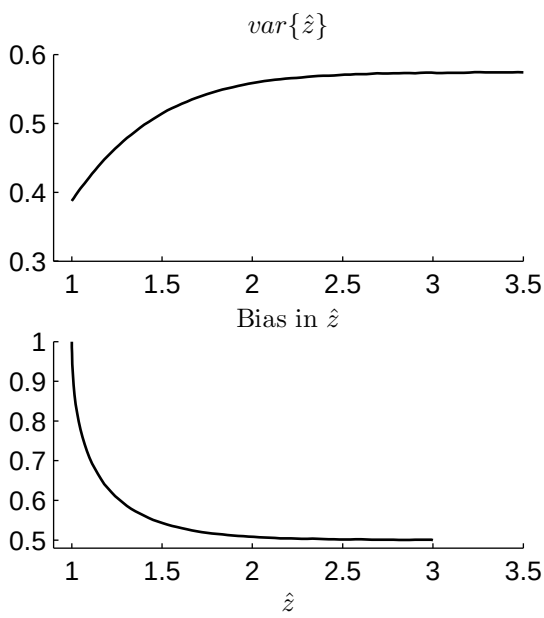

Figure 1. Plot of $var\{\hat{z}\}$ and bias against $\hat{z}$. Results of Monte-Carlo study to determine (Top) variance, and (Bottom) bias of $\hat{z}$. Results are plotted against $\hat{z}$. See text for details.

The bias and variance are plotted against the estimated value of z (figure 1). When applied in practice the variance has to be derived from the estimated value of z, as the true (target) values will be unknown. The target range, $0 \leq z \leq 3$, is therefore mapped to an estimated range $1 \leq \hat{z} \leq 3.5$. The z-tracker estimation procedure uses the values in figure 1 stored in two look up tables, one for r_l and one for bias correction. The scalar value of r_l used for each segment is achieved by using the mean of $\hat{z}$ over the frequencies of interest. Bias correction is applied as a final step after filtering or smoothing with bias applied separately at each frequency in the z-domain.

2.4. Morse wavelet coherence

The z-tracker estimates are compared against Morse wavelet coherence estimates applied to the same data. The Morse wavelet estimates are constructed as described in [8]. The two processes, (x, y) are subject to continuous wavelet transform (CWT) using a pre-specified number, K, of orthogonal Morse wavelets at each scale. No segmentation of the data is required for CWT analysis, in contrast to the segmentation required for the z-tracker. In this study we use $K = 5$ and $K = 10$. The value $K = 10$ is typical of that used in Morse wavelet analysis [17] and is similar to the complex degrees of freedom that can be achieved with temporal smoothing in Morlet wavelet coherence estimates [18]. In [8] $K = 9$ was used in analysis of intracellular recordings. Including estimates with $K = 5$ allows the effects of different levels of smoothing to be assessed. Morse wavelet parameters are $\beta = 9$ and $\gamma = 3$, as recommended in [30]. Scales for analysis are specified logarithmically as a number per octave, in this study we use 6 scales/octave, specified as a maximum scale (minimum frequency) and number of octaves.

3. Results

3.1. Surrogate data

The performance of the z-tracker is assessed using surrogate data. The surrogate data has coherence which is constant across frequencies and varies over time. The two signals are generated using the model in [19] as

$$x_t = \xi_t \tag{10}$$

$$y_t = \beta_t x_t + d_t \varepsilon_t \tag{11}$$

where ξ_t and ε_t are independent white noise processes with zero mean and unit variance. The target time varying coherence is $|\gamma_{xy;t}(\lambda)|^2 = 1 - \frac{d_t^2}{\beta_t^2 + d_t^2}$ [19]. For target coherence in the range $[0, 1]$, the coefficients to generate the surrogate data are

$$\beta_t = \gamma_{xy;t}(\lambda) \tag{12}$$

$$d_t = \sqrt{1 - |\gamma_{xy;t}(\lambda)|^2}. \tag{13}$$

As defined in equations 10 and 11, x_t is a discrete time second-order stationary process with unit variance at all t, and y_t is a sigma-oscillatory process formed from the sum of two uniformly modulated processes.

We consider three forms of target coherence 1) Linear increase and decrease over range [0,1] with time scale 20 seconds, 2) Linear increase and decrease over [0,1] with time scale 2 seconds, and 3) Linear increase with the same increment per time step as in 1) with randomly occurring step decreases in coherence, from values above $|\gamma_{xy;t}(\lambda)|^2 = 0.8$ to values below $|\gamma_{xy;t}(\lambda)|^2 = 0.2$. These scenarios are chosen to investigate different aspects in the performance of the z-tracker. Scenario 1) has slow time-varying coherence representing a situation where we would expect the z-tracker to perform well. Scenario 2) has coherence varying over a much more rapid time scale, which may represent more of a challenge for the z-tracker. Scenario 3) combines time varying coherence over the same time-frame as 1) with sudden changes, we would expect the adaptive nature of the estimator to cope well with these occasional changes and would expect a similar level of performance to scenario 1).

Data for each scenario is generated using equations 10, 11. Scenarios 1) and 2) use a total of 200000 time points for each trial, this is equivalent to 200 seconds at the assumed sampling rate of 1 ms. Scenario 3) generates data over 10 ramp sections with timings for each step decrease determined randomly, the example presented here uses 86589 time points, or 86.5 seconds. For each configuration 100 repeat trials are generated and, unless stated, metrics are aggregated over these 100 trials.

3.2. Scenario 1. Twenty second linear increase-decrease in target coherence.

Figure 2 shows the target and estimated coherence for three estimates: 1) z-tracker with $\alpha = 0.1$, $T = 128$, tracking only, 2) z-tracker $\alpha = 0.9$, $T = 128$ with smoothing, and 3) MWT coherence with $K = 10$ using 6 scales per octave over the frequency range $[8, 256]$ Hz, a total of 31 scales. Z-tracker estimates are averaged over 31 frequencies covering the first half of the frequency range $[7.8, 250]$ Hz, the MWT estimate is averaged over all 31 scales. The time for the z-tracker estimate for each segment is assigned as the centre point of each segment. The same temporal decimation is used for plotting the MWT estimate. Thus, both z-tracker and MWT coherence estimates have the same frequencies in their respective averages and use the same number of time points. Also included are the upper and lower 95% point-wise confidence limits. Averaging for coherence and confidence limits is done in the z-domain. The choice of $\alpha = 0.1$, tracking and $\alpha = 0.9$, smoothing represent the two extremes in terms of the level of smoothing applied to the single segment coherence estimates. Qualitatively the additional smoothing in the latter estimate is clear in figure 2. Also visible in the tracking only estimate is the lag introduced by the Kalman filter, the estimated coherence can lag slightly behind the target coherence in figure 2 (top).

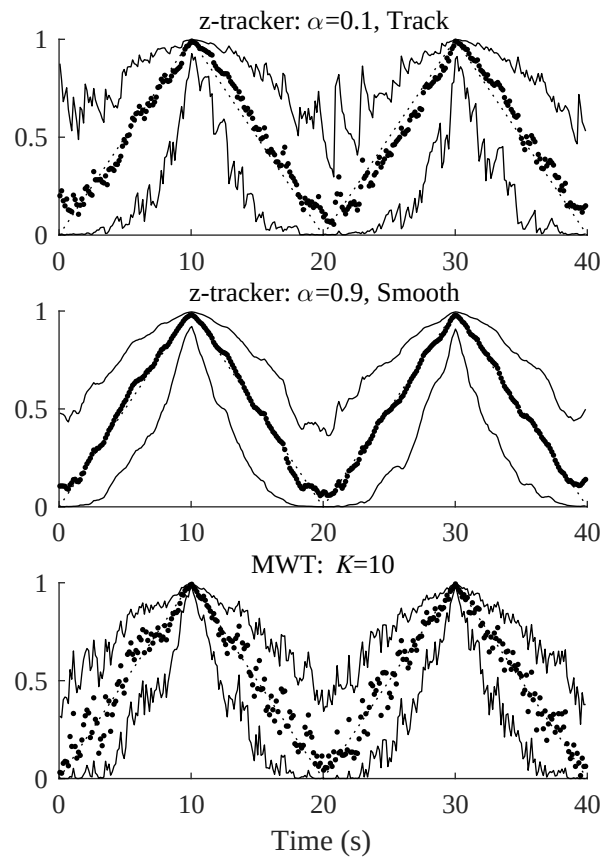

Figure 2. Single trial coherence estimates with target coherence modulated over range [0 1] with 20 second time scale. Estimates shown for 40 of the 200 seconds. (Top) z-tracker estimate $\alpha = 0.1$, $T = 128$, tracking only, averaged using 31 frequencies over range $[7.8, 250]$ Hz. (Middle) z-tracker estimate $\alpha = 0.9$, $T = 128$, smoothed and averaged over same frequency range. (Lower) Multiwavelet estimate with $K = 10$ averaged using 31 scales over frequency range $[8, 256]$ Hz at 6 scales/octave. In all cases small dots and large dots indicate target and estimated coherence for each time point, respectively. Solid lines are average upper and lower point-wise confidence limits for estimates.

The three estimates in figure 2 all capture the modulation of coherence over the 20 second time scale using an average over half of the full frequency range. Such extensive averaging in neurophysiological signal analysis is not that common. Figure 3, using the same layout and parameters as figure 1, shows the coherence estimates for a single frequency, using the median frequency for both the z-tracker and MWT estimates. While less reliable than the estimates incorporating averaging over frequencies these single

frequency estimates still capture the modulation of the target coherence over the 20 second time frame.

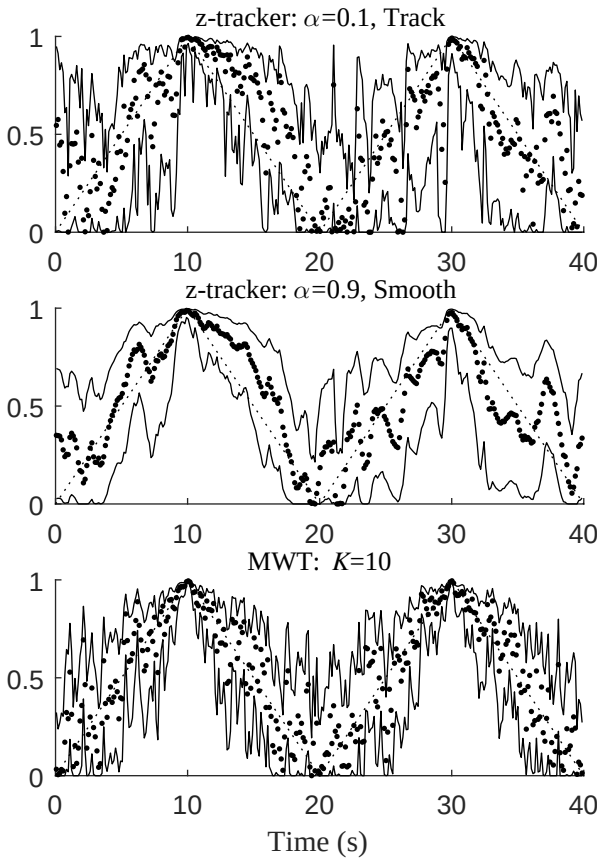

Figure 3. Single trial, single frequency coherence estimates for 20 second coherence modulation. Same layout and parameters as figure 2.

The performance of the z-tracker is quantified using an MSD metric calculated from the estimated and target coherence at each time point. First we consider the effect of changing the segment length T. Figure 4 shows boxplots of the MSD, generated as a single MSD measure for each of the 100 trials from the z-tracker coherence estimate averaged over all frequencies and over all segments. Box plots are shown using a standard layout [32], with boxes extending from the 25th to 75th percentiles and a horizontal line at the median. Vertical lines with whiskers indicate the extremes of the data. Individual outliers are shown as $'+'$. Notches are included which indicate approximate 95% confidence limits for the median, allowing visual comparison of different configurations.

It is clear that the MSD decreases monotonically as T reduces. Thus, for the broad-band target coherence in this example, frequency resolution can be sacrificed to obtain a more accurate estimate using shorter segment lengths. We did not consider segment lengths smaller than $T = 128$, the frequency resolution

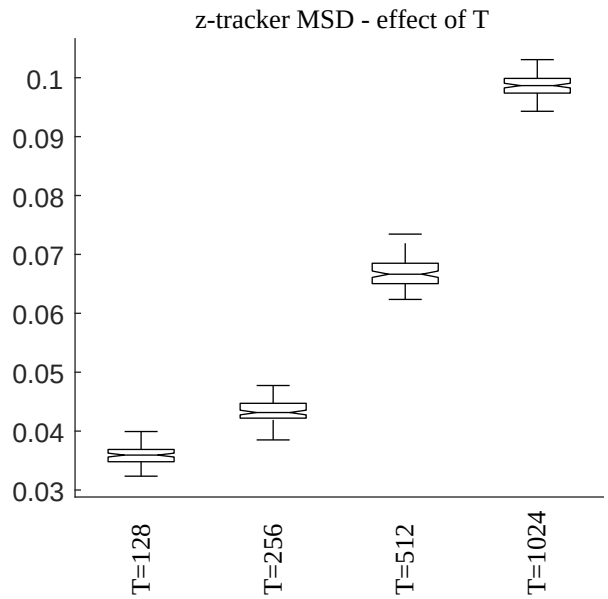

Figure 4. Box plots of the MSD between target and estimated coherence for the z-tracker applied to the 20 second ramp increase/decrease data. Other parameters are $\alpha = 0.9$ with smoothed estimates. Box plots constructed from 100 repeats with MSD calculated for average over all frequencies and over all segments for each trial.

for the assumed sampling rate of 1000/sec is ~ 8 Hz, which is towards the upper end of that typically used in Fourier based analyses of neurophysiological data.

Next we consider a fixed segment length, $T = 128$, and look at the effects of varying α in equation 7. The range of values is $0 < \alpha < 1$, we use the four values 0.1, 0.37, 0.61, 0.9. Low values of α give greater weight to the instantaneous process noise, making the filter more responsive to the residual error. Larger values of α give greater weight to previous data providing more smoothing. The intermediate values represent time constants of 1 and 2 time bins respectively in the exponential smoothing applied in equation 7.

Figure 5 shows the MSD for the z-tracker using these four values of α for tracking and smoothing, and the MSD for MWT estimates using $K = 5$ and $K = 10$. The MSD for each trial is calculated as the average coherence over the same 31 frequencies/scales as used in figure 2 and over all 1562 segments. A number of conclusions can be drawn from figure 5. The MSD for smoothed z-tracker estimates is around 37% smaller than that for the tracking based estimate for the same value of α. There is a steady improvement in MSD as the value of α increases for both tracked and smoothed z-tracker estimates. The MSD for MWT improves considerably for $K = 10$ compared to $K = 5$, the MSD for $K = 10$ is comparable to that for the tracked MSD estimates. For this data the lowest MSD is obtained using the z-tracker with configuration $T = 128$, $\alpha = 0.9$

with smoothed estimate. This has an MSD that is around 40% smaller than the MWT estimate with $K = 10$.

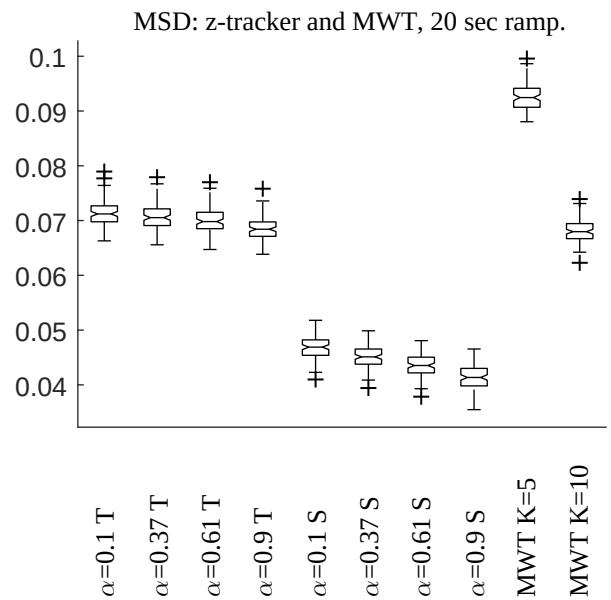

Figure 5. Box plots of the MSD between target and estimated coherence for z-tracker and MWT coherence estimates applied to the 20 second ramp increase/decrease data. Other parameters are $T = 128$ for the z-tracker and $K = 5$, $K = 10$ for the MWT estimates. Box plots constructed from 100 repeats with MSD calculated for average over 31 frequencies/scales for the z-tracker/MWT and over all 1562 segments for each trial. MSD shown for four values of α, with the suffix T indicating tracking and the suffix S indicating smoothing.

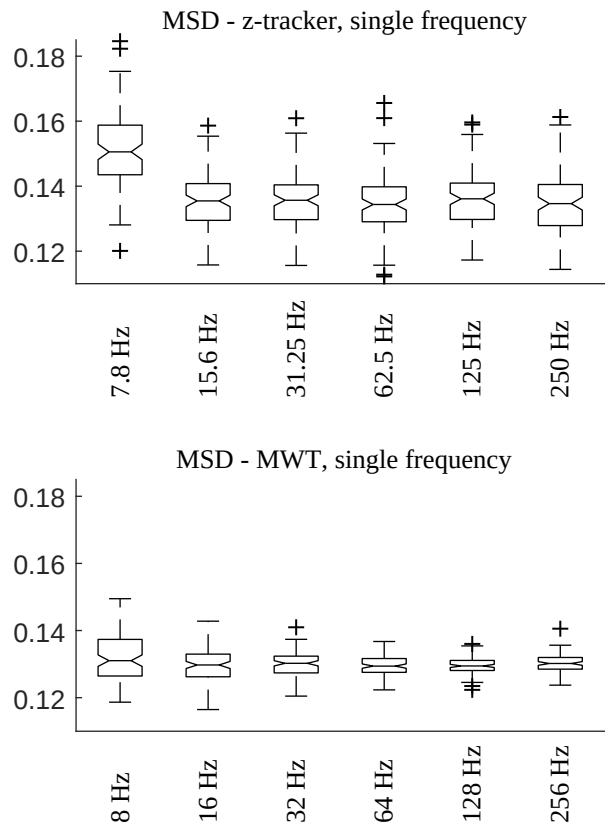

Figure 6. Single frequency MSD box plots for (Upper) z-tracker, and (Lower) MWT coherence estimates applied to the 20 second ramp increase/decrease data. For the z-tracker $T = 128$, $\alpha = 0.9$, with smoothing. For MWT estimates $K = 10$. Box plots constructed from 100 repeats with MSD calculated for individual frequencies using average over all 1562 segments/time points for each trial. MSD shown using same vertical axes.

Single frequency MSD plots are shown in figure 6 for z-tracker with $T = 128$, $\alpha = 0.9$ with smoothing and for MWT with $K = 10$. Frequency dependent effects can be seen for both types of estimate, the MSD is larger for the lowest frequency shown in the z-tracker, this is also the fundamental frequency in the single segment multi-taper coherence estimates. For MWT estimates the MSD tends to have smaller variability as the frequency increases. The single frequency MSD for the MWT estimate is around 7% lower than that for the z-tracker.

3.3. Scenario 2. Two second linear increase-decrease in target coherence.

This section describes a similar analysis to section 3.2 applied to surrogate data using a 2 second cycle time for the linear increase and decrease in the target coherence. Each trial has 200000 data points, assumed duration 200 seconds, which includes 100 repetitions of the two second triangular coherence modulation. Figure 7 shows z-tracker and MWT coherence estimates over the first 10 seconds using averaging over frequencies with the same parameters and layout as figure 2. Figure 8 shows single frequency plots using the same layout as figure 3.

MSD box plots using the average across frequencies are shown in figure 9 using the same parameters and layout as figure 5. MSD box plots for single frequencies are shown in figure 10 using the same parameters and layout as figure 6.

The z-tracker does not perform as well on scenario 2. This is due to the more rapid modulation of the target coherence with only 15 segments for each 2 second modulation window. In figures 7 and 8 both tracking and smoothing z-tracker estimates detect the modulation of coherence over the 2 second time window. The smoothed estimate in figure 7(centre) has a reduced range of coherence values compared to the MWT estimate, suggesting the z-tracker may be applying too much smoothing for this data. The confidence band for the single frequency z-tracker estimate with smoothing, figure 8(centre) appears to have wider point-wise confidence intervals than those for the MWT estimate. Quantitatively the MWT

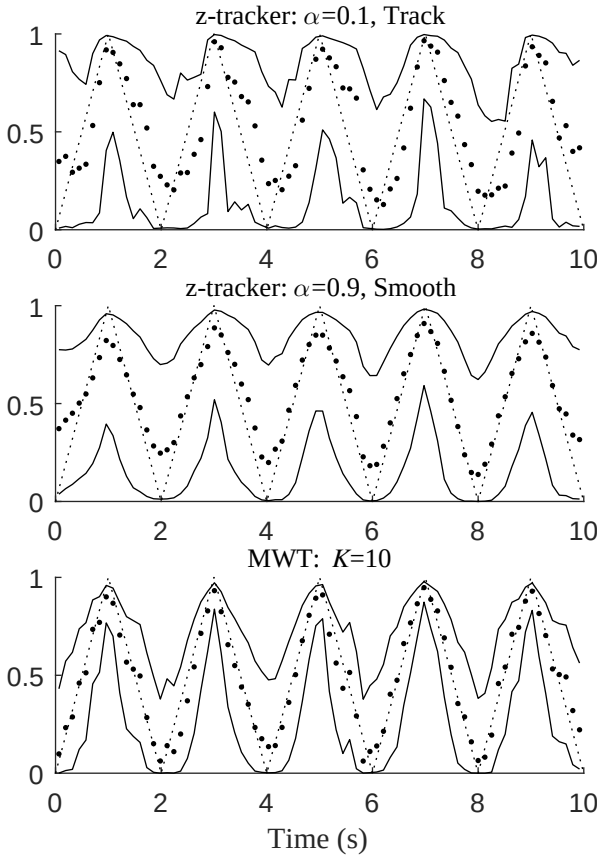

Figure 7. Single trial coherence estimates with target coherence modulated over range [0 1] with 2 second time scale, averaged over frequencies. Estimates shown for 10 of the 200 seconds. Parameters and layout same as figure 2.

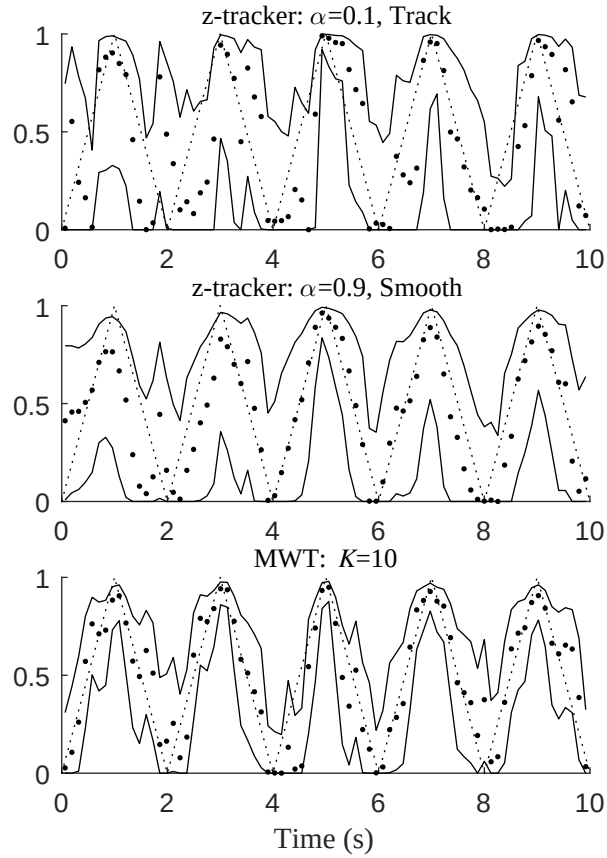

Figure 8. Single trial, single frequency coherence estimates for 2 second coherence modulation. Same layout and parameters as figure 3.

has a lower MSD than the z-tracker (figure 9), the MWT estimate with $K = 10$ has an MSD that is 23% lower than the z-tracker with $\alpha = 0.9$ with smoothing. The MSD values are larger (160% for z-tracker; 21% for MWT) than those for scenario 1 in figure 5. The MWT estimate has a clear frequency dependent effect for single frequency MSD metrics, figure 10 (lower), reflecting the scale dependent time-frequency bandwidths of the continuous wavelets. The single frequency MSD for the z-tracker, figure 10 (upper), is similar to scenario 1 in terms of any frequency dependency.

3.4. Scenario 3. Linear increase and step decrease in target coherence.

This scenario considers the ability of the z-tracker and MWT estimates to detect changes in coherence over different time scales. In this case the target coherence consists of slow increases and step decreases. The increase has the same rate of change as in scenario 1, the step decrease occurs over 1 time step, 1 ms. The transition points are determined randomly, with a

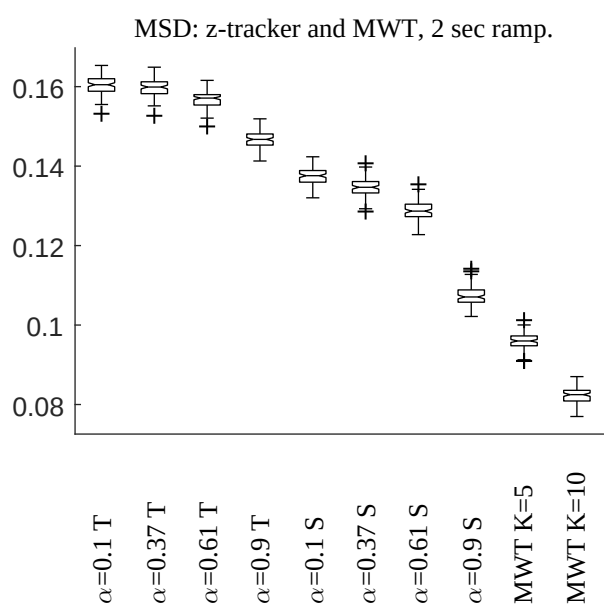

Figure 9. Box plots of the MSD between target and estimated coherence for z-tracker and MWT coherence estimates applied to the 2 second ramp increase/decrease data with averaging across frequencies. Same layout and parameters as figure 5.

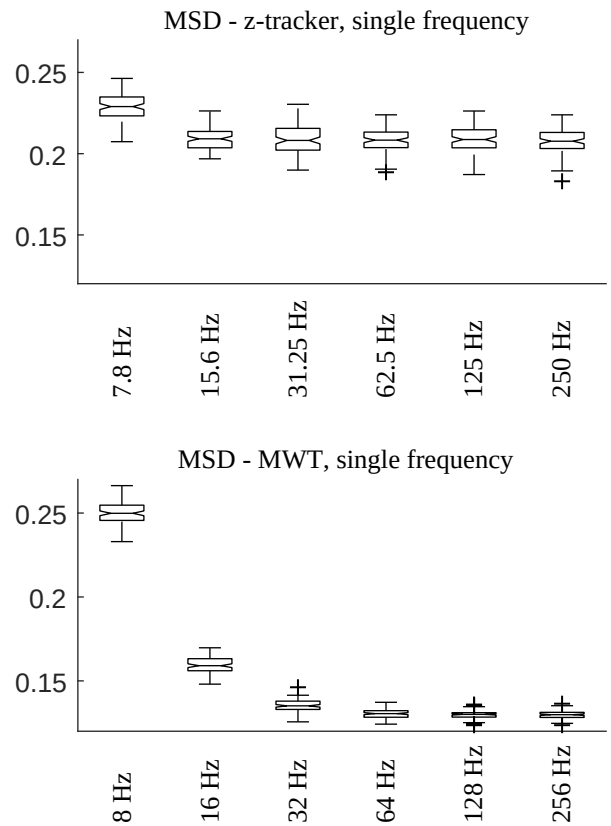

Figure 10. Box plots of the MSD between target and estimated coherence for z-tracker and MWT coherence estimates applied to the 2 second ramp increase/decrease data for single frequencies. Same layout and parameters as figure 6. MSD shown using same vertical axes plotting.

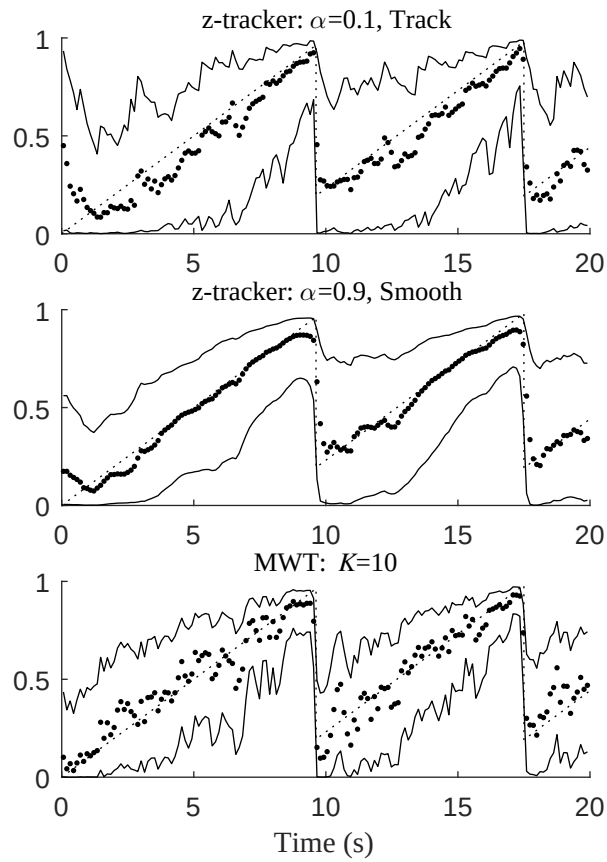

Figure 11. Single trial coherence estimates with coherence modulated with slow increase and step decrease with averaging across frequencies. The increase in target coherence has the same rate as scenario 1, figure 2, the step decrease occurs over 1 time step, 1 ms. Parameters and layout same as figure 2.

uniform distribution in target coherence of $[0.8, 1.0]$ for the end of the ramp and $[0, 0.2]$ for the end of the step decrease. Each trial contains 10 repetitions with 86588 data points, 86.6 seconds. Figure 11 shows z-tracker and coherence estimates for 20 seconds from one trial using averaging over frequencies. The z-tracker and wavelet estimates both capture the slow increase and sudden decrease in target coherence. The smoothing over segments in the z-tracker estimate, with $\alpha = 0.9$ can be seen prior to the onset of the step decrease.

MSD metrics, calculated using the same approach as scenarios 1 and 2 from 100 trials, are shown in figure 12. These indicate that the z-tracker, with smoothing, has lower MSD than the MWT estimates, and for this configuration a lower value of α can reduce the MSD. A lower value of α is likely to improve the performance of the z-tracker around the step changes in the target coherence.

3.5. Using P_l to characterize the variability of z-tracker estimates.

The coherence estimates in figures 2-3, 7-8, 11 include point-wise confidence limits. These help characterise the variability associated with different estimates. For the z-tracker confidence limits are derived from the Kalman filter output, equation 9. This section examines how P_l changes with the different z-tracker configurations for scenario 1, and compares the Kalman filter error P_l with $var\{\hat{z}\}$ for the two MWT estimates. Figure 13 shows box plots of the median P_l for the 8 configurations of the z-tracker used on scenario 1, for each of the 100 trials a single P_l, the median, is used. These show that, as might be expected, the error is reduced for smoothing compared to tracking. For comparison the fixed values of $var\{\hat{z}\}$ for the two MWT estimates are included, these suggest the variability in tracking estimates is similar to that for the MWT estimate with $K = 5$, whereas the variability in smoothing estimates is similar to an MWT estimate with $K = 10$.

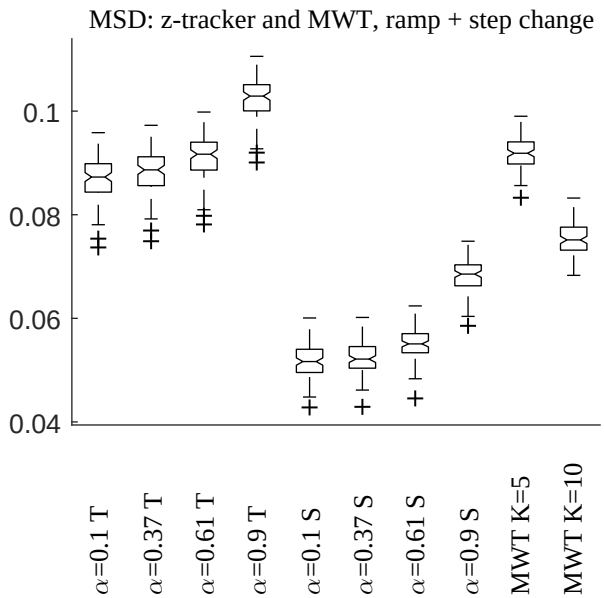

Figure 12. Box plots of the MSD between target and estimated coherence for z-tracker and MWT coherence estimates applied to the slow ramp increase and step decrease data with averaging across frequencies. Same layout and parameters as figure 5.

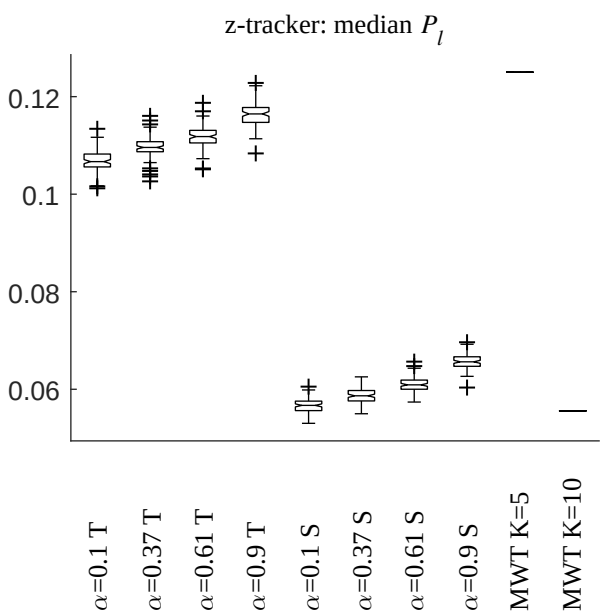

Figure 13. Box plots of the median P_l for the 100 repeat runs in scenario 1 using the 20 second ramp increase/decrease in target coherence. Horizontal lines for the MWT estimates show the fixed values of $var\{\hat{z}\}$ for $K = 5$ and $K = 10$.

Using a single value of P_l to represent the variability for each run does not provide any information regarding the distribution across segments in each trial. Figure 14 shows a histogram of the distribution of P_l for a single trial in scenario 1 across the 1562 segments with $T = 128$ and $\alpha = 0.9$ with smoothing. The distribution has a positive skew, this is likely to reflect the adaptive nature of the Kalman filtering. When a large residual triggers an increase in the filter gain the error will also increase transiently. For the MWT estimate with $K = 10$, $var\{\hat{z}\} = 0.56$, this is close to the peak in the distribution of P_l.

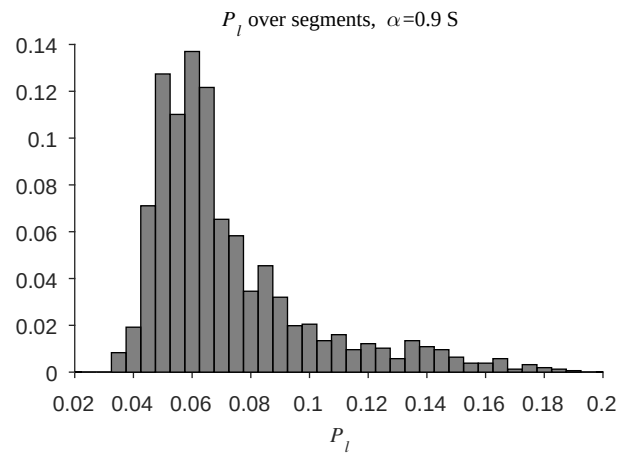

Figure 14. Normalised histogram of P_l over 1562 segments in a single trial for scenario 1 with configuration $\alpha = 0.9$, smoothing. The value of $var\{\hat{z}\}$ for the MWT estimate with $K = 10$ is 0.56.

3.6. Testing for zero coherence.

An important aspect of coherence analysis is testing for a null hypothesis of zero coherence. In this section we examine the behaviour of the z-tracker when applied to surrogate data with no correlation. Simulated data of length 200000 samples, assumed sampling rate 1 ms, generated using equations 10, 11 with $\beta_t = 0$ and $d_t = 1$ gives a target coherence of zero, for all frequencies. Figure 15 compares the z-tracker coherence estimate, $T = 128$ $\alpha = 0.9$ using smoothing, with the MWT estimate using $K = 10$ for a single trial, with coherence averaged over 31 frequencies covering the same frequency range in both cases. For comparison both plots have 80% of average coherence values less than 0.1. Indicative single frequency estimates are shown in figure 16, using the median frequency value for each estimate. The horizontal lines are the upper 95% confidence limit for each estimate, the value of 0.33 for the z-tracker was determined empirically using 100 repeat runs and estimating the confidence limit from the 5% point of the distribution taken across repeat runs and across frequencies. The confidence

limit for the MWT estimate uses the expression in [8]. Both estimates exhibit a similar range of values, with no obvious bias over time from the z-tracker estimate.

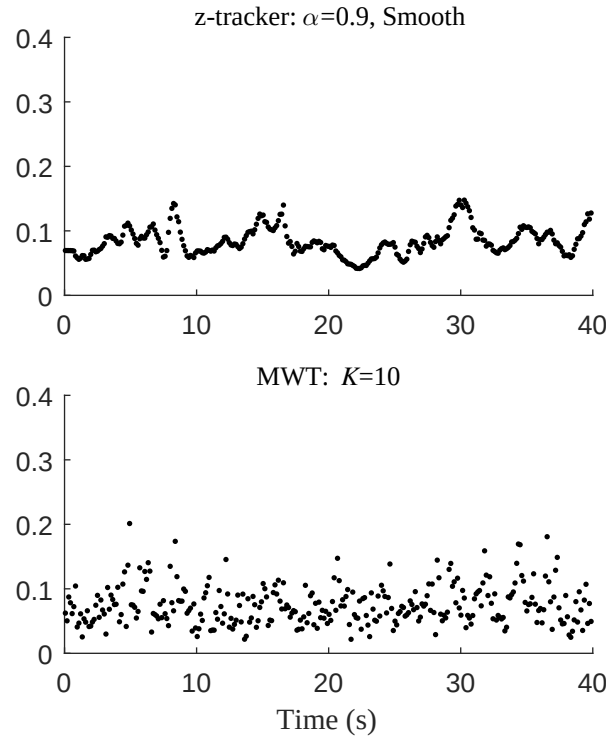

Figure 15. Single trial z-tracker ($T = 128$, $\alpha = 0.9$ with smoothing) and MWT ($K = 10$) coherence estimates for uncorrelated stationary Gaussian data. Estimates are averaged over 31 frequencies, using the same frequencies as figure 2.

Determined empirically for each z-tracker configuration, using the approach of taking the 5% point of the distribution of estimated coherence values across 100 repeat runs and across all frequencies, gives a range of values for the 95% confidence limit of 0.475 for $T = 128$, $\alpha = 0.1$ with tracking to 0.25 form $T = 1024$, $\alpha = 0.9$ with smoothing. These empirical confidence limits decrease as T is increased and as α is increased and are lower for smoothing than tracking. For comparison using the expression in [8] to determine confidence limits, using the complex degrees of freedom for each MWT estimates give 95% confidence limits of 0.53 for $K = 5$ and 0.28 for $K = 10$. Although expressions to estimate the complex degrees of freedom of the z-tracker have not been developed, this comparison suggests that the two approaches, with parameter values as used in the present study, have similar ranges for their complex degrees of freedom.

To quantify the relative performance of the z-tracker against the benchmark MWT estimate, figure 17 shows boxplots of MSD estimates generated as a single MSD measure for each of the 100 trials for two z-tracker estimates ($T = 128$ and $T = 1024$, both with $\alpha = 0.9$) and two MWT ($K = 5$ and $K = 10$) estimates.

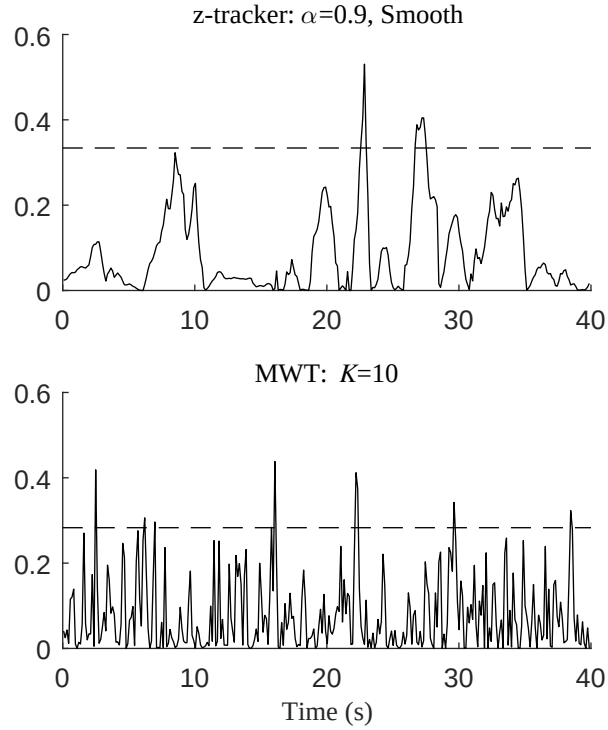

Figure 16. Indicative single frequency coherence estimates, using the median frequency for the same data and same analysis parameters as in figure 16. Upper trace is z-tracker estimate, Lower trace is MWT estimate. The horizontal dashed lines are the upper 95% confidence limits for a null hypothesis of uncorrelated data, determined empirically for the z-tracker and using the expression in [8] for the MWT estimate.

The box plots in figure 17 suggest that the performance of the z-tracker on uncorrelated data is similar to that of MWT based estimates. For this data a longer segment length leads to lower MSD values for the z-tracker.

3.7. Experimental data.

This section illustrates application of the z-tracker to local field potentials (LFP) recorded from the medial prefrontal cortex (mPFC) and basolateral amygdala (BLA) in anaesthetised rat as part of a study investigating neural interactions in response to systemic application of a benzodiazepine receptor partial inverse agonist which mimics stress responses. The data and comparative analysis of coupling between the two LFPs before and after application of the agonist is described in [45]. Here we analyse the correlation between the two LFP signals over 990 seconds of data which starts ~ 3.5 minutes before the injection of the first dose of the agonist (a total of 4 doses were administered). Using ordinary coherence

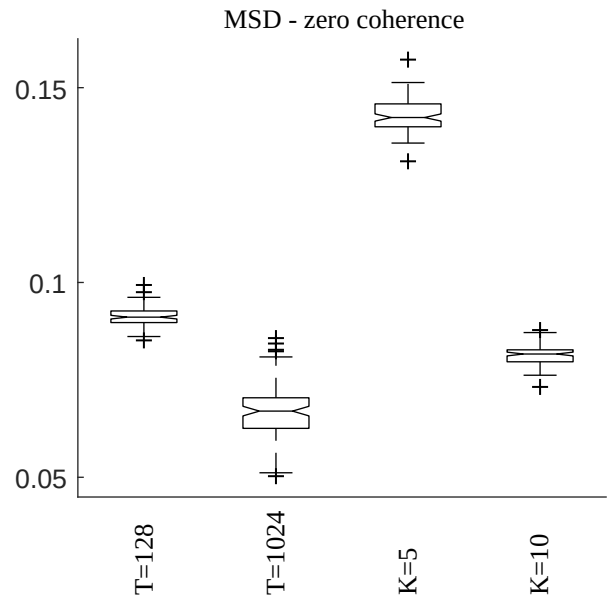

Figure 17. Box plots of the MSD for target coherence of zero for two z-tracker ($T = 128$ and $T = 1024$) and two MWT ($K = 5$ and $K = 10$) coherence estimates. Other parameters are $\alpha = 0.9$ with smoothing for the z-tracker estimates. Box plots constructed from 100 repeats with MSD calculated for average over 31 frequencies/scales for the z-tracker/MWT and over all 1562 segments for $T = 128$ z-tracker and over all 195 segments for $T = 1024$ z-tracker. MSD for MWT use 195 time points matching the midpoint of segments for the $T = 1024$ z-tracker.

estimates it was found that the mPFC-BLA coherence after the final dose was significantly lower than the coherence prior to the first dose at frequencies <2Hz [45]. The aim in applying the z-tracker to this data is to get additional insight into the time scales of these changes in coherence. Figure 18 shows the z-tracker coherence estimate over the 990 second record with configuration $T = 1024$, $\alpha = 0.9$ with smoothing. The choice of T is motivated by the need to examine frequencies <2Hz, and the choice of α is motivated by the MSD results in figure 5.

A reduction in the coherence after the first dose of the agonist can be seen in the heat map in figure 18(Upper). The section at frequency 0.98Hz, the lowest frequency bin, figure 18(Lower), quantifies this change over time. Following each dose of the agonist there is a marked reduction in coherence, this is most prominent following the first dose, when the coherence is abolished around 330 seconds. Following the final dose there is no obvious reduction in coherence. Prior to the first dose the mean coherence at 1 Hz is 0.78, the mean coherence from 60 seconds after the last dose until the end of the record is 0.64. Thus, for this example, the z-tracker is able to give additional insight into changes in coherence over time, and appears to detect changes in single frequency components, figure 18(Lower).

3.8. Computational complexity of z-tracker and multiwavelet algorithms.

One factor in the choice of algorithm to use to estimate time-varying coherence is the computational complexity of the different approaches. Here we consider briefly the computation time of the two methods, focusing on a comparison of the time to compute the necessary Fourier transforms using an FFT algorithm, and using a comparison of the run time on the same data.

The algorithms are implemented in MATLAB [31], which uses an FFT algorithm with computing time of order $O(N \log N)$ for an FFT with N points, this is independent of the value of N [22]. Using this expression we can compare the computational time to compute the Fourier coefficients for the z-tracker and MWT algorithms. The MWT algorithm uses an FFT based convolution to calculate the wavelet coefficients at each scale, this is achieved with an inverse Fourier transform, we assume the computation time for forward and inverse Fourier transforms is the same. The following comparison is based on scenario 1, section 3.2, which uses bivariate data of length 2×10^5 points. Considering the z-tracker with segment size $T = 128$ and $L = 1562$ segments, a bivariate analysis for single segment coherence estimates with $K = 2$ multitaper windows will have computing time of order $O\left(4\,L\,T\,\log T\right) = O\left(3.9 \times 10^6\right)$. The MWT estimate, using $K = 10$ orthogonal Morse wavelets applied to the complete record $N = 2 \times 10^5$ using $N_s = 31$ scales will require Fourier transforms with computing time of order $O\left(2N_s\,(K+1)\,N\,\log N\right) = O\left(1.6 \times 10^9\right)$. These figures suggest that the z-tracker will be 2-3 orders of magnitude faster in execution time than the multiwavelet analysis. However, the z-tracker has a number of additional steps that must be performed for each segment according to the algorithm in section 2.2. In a comparison of execution times in MATLAB, comparing 100 runs on scenario 1 data, the z-tracker is about 50 times faster than the multiwavelet analysis. Thus, if execution time is an important factor in any analysis the z-tracker may be preferred to multiwavelet analysis.

4. Discussion

This paper has introduced the z-tracker algorithm for estimating coherence in segmented bivariate data with large numbers of segments. The method combines multi-taper spectral estimates with Kalman filtering/smoothing to estimate coherence locally for each segment using a combination of multiple windows and local smoothing over segments. The Kalman filter uses adaptive filtering [25] where the process noise variance, q_l, is inflated in response to larger

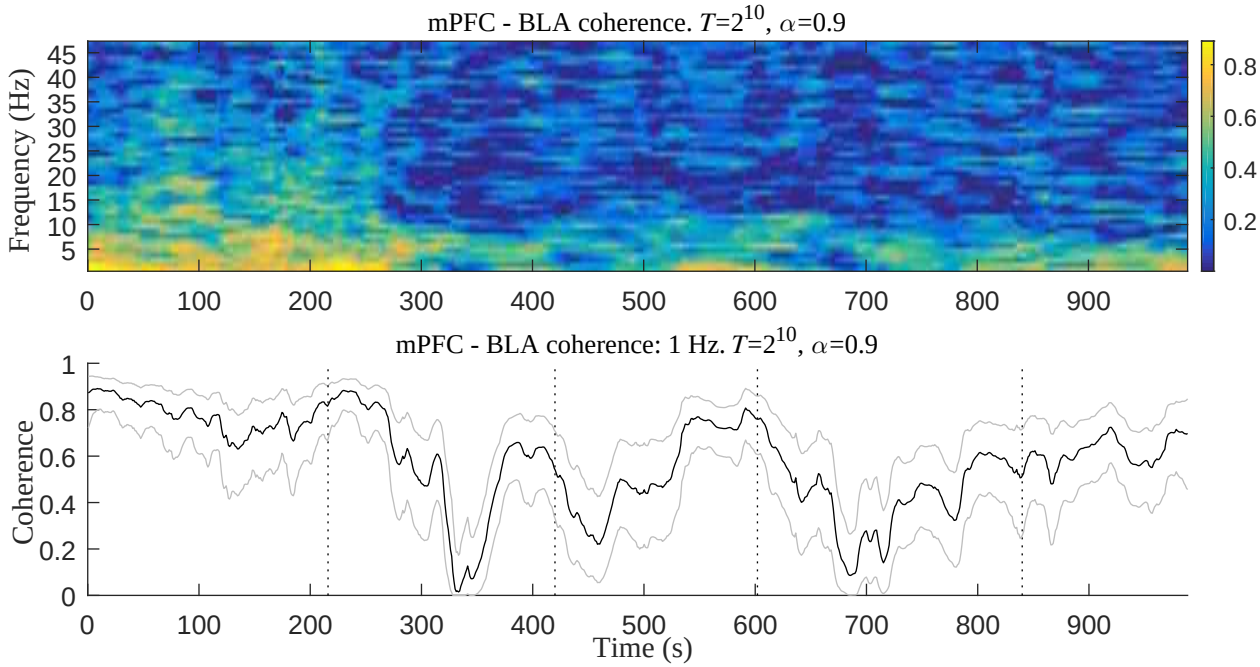

Figure 18. Analysis of *in-vivo* recording of local field potentials from mPFC and BLA in anaesthetized rat during an experiment to mimic increased stress pharmacologically. Four doses of a stress agent were applied at 216, 420, 602 and 840 seconds into the recording. (Upper) Heat map of z-tracker coherence estimate over the 990 second record, $T = 1024$, $\alpha = 0.9$ with smoothing, using 966 segments. Colour bar to the right indicates coherence magnitude. (Lower) Section with coherence estimate at lowest frequency bin, 0.98 Hz. Solid line indicates coherence estimate, grey lines are upper and lower 95% point-wise confidence limits. Vertical dotted lines indicate times at which stress agent was administered.

than expected residual terms. This allows the filter to respond rapidly to sudden increases or decreases in the correlation. In contrast if the correlation is relatively constant or slowly changing the Kalman filter can apply greater levels of local smoothing, helping to reduce variability.

The performance of the z-tracker was explored using surrogate data and compared with wavelet coherence using an MSD metric. For data with slowly varying target coherence, including occasional step changes, the z-tracker exhibited a lower MSD than MWT coherence. For more rapidly changing target coherence a MWT estimate gave a lower MSD than the z-tracker. The two parameters to consider in a z-tracker analysis are the segment size, T, and the smoothing to apply to the Kalman filter noise sequence, using parameter α, with larger α resulting in greater smoothing. Using shorter segment sizes reduced the MSD as did a larger value of α. An exception to this was data with sudden changes in coherence, when a smaller value of α gave a lower MSD. In addition, when testing for zero coherence increasing the segment size reduced the MSD. Analysis of *in vivo* experimental LFP data demonstrated the potential of the method to provide insight into modulation of coherence over time.

To our knowledge this is the first attempt at combining multi-taper spectral estimates with adaptive Kalman filtering to estimate correlation over time. It builds on our earlier work using adaptive Kalman filtering in the univariate case for spectral estimation [10] and non-adaptive Kalman filtering with Periodogram based spectral estimates. Auto and cross spectral estimates were tracked separately over segments with Kalman filtering/smoothing, and combined to estimate coherence for each segment [9]. The advantage of the z-tracker is that only a single set of frequency components are used in the Kalman filtering step. In addition the assumption of constant variance for the log_e of the real and imaginary components of the cross spectrum used in [9] apply only when the coherence is zero, this may introduce an additional bias into estimates which have non-zero coherence. This does not apply to the z-tracker which instead works with a single set of frequency values in the z domain.

Several aspects of the z-tracker are worthy of further study. We have used only one configuration for estimation of the single segment coherence estimates in equation 3, with $NW = 1.5$, $K = 2$, the bias and variance lookup tables apply only to this case. Further lookup tables could be generated for increased K to give added flexibility. The ability of the z-tracker to respond to rapidly changing coherence between

segments uses increased process noise variance to increase the Kalman gain, this is triggered by larger than expected residual, equation 6. In the estimation of q_l' we used all frequency points (apart from zero and nyquist), in some cases it may be more appropriate to use a restricted range of points to estimate the residual variance.

This study considers only time series data. Extending the approach to point-process data would open up further applications in, for example, analysis of multielectrode array recordings of single unit data. A possible route here would be to consider the approach to point-process analysis in [24], which allows analysis of time series and point process data in a combined framework.

The z-tracker uses an empirical approach in the z-domain with coherence estimates and point-wise confidence limits derived from the Kalman filter output. Confidence limits for a null hypothesis of zero coherence are derived empirically using mote-carlo methods. The success of the method will rely, in part, on the accuracy of the assumptions made regarding the applicability of the Kalman filter in the z-domain. Comparison with the multiwavelet coherence suggests these assumptions are reasonable. One advantage of wavelet coherence is the theoretical work which has derived expressions for the statistical distribution facilitating hypothesis testing [17]. Further work is required to develop a similar level of statistical rigour for the z-tracker. A possible approach is to re-formulate the z-tracker as a weighted overlapping segment average (WOSA) estimate, as used for temporally smoothed wavelet coherence estimates [18]. Our recommendations for the choice of z-tracker parameter α are based on an MSD metric. An alternative theoretical treatment could consider a likelihood expansion of the Kalman filter state and observation models to choose α using maximum likelihood over the range for α, e.g. [37].

The z-tracker provides a computationally efficient approach, around 50 times faster in our MATLAB implementation, for analysis of correlation in long records which can be sectioned into short segments. Applications include comparison of baseline activity vs stimulus-induced changes in activity as in figure 18. The method is also suitable for more exploratory analyses, for example investigating the consistency of correlation over time. In experiments involving repeat trials over time the method could be used to characterise changes in coherence from trial-to-trial, with the Kalman filter error used to quantify the uncertainty across trials. The data adaptive nature of the algorithm should also open up new approaches in coherence estimation for non-stationary data in other fields.

5. Software toolbox

A software toolbox in MATLAB to undertake the analysis in this paper is freely available at `http://www.neurospec.org/`. The software includes a user guide and example scripts.

Acknowledgments

The authors would like to thank the referees for their helpful comments. The work of D.M. Halliday and J-S. Brittain was supported by the Biotechnology and Biological Sciences Research Council of the United Kingdom (Ref 10477).

Appendix A. Kalman filtering and smoothing.

This Appendix provides an overview of the Kalman filtering and smoothing equations as applied to the single segment coherence estimates. The Kalman filter state and observation equations are [11, 26]

$$\mathbf{x}_{l+1} = \boldsymbol{\phi}_l \mathbf{x}_l + \mathbf{w}_l, \tag{A.1}$$

$$\mathbf{z}_l = \mathbf{H}_l \mathbf{x}_l + \mathbf{v}_l. \tag{A.2}$$

Here $\mathbf{x}_l$ is the (unknown) vector of z-transformed coherence at segment l and $\mathbf{z}_l$ is the vector containing the single segment z-transformed estimate, equation 4, over the frequency range of interest. The vectors $\mathbf{w}_l$ and $\mathbf{v}_l$ are the process and observation noise with covariance matrices $\mathbf{Q}_l$ and $\mathbf{R}_l$, respectively. A number of assumptions are made concerning the characteristics of the state transition and observation matrices and the noise processes. As in our previous work [9, 10] we set $\boldsymbol{\phi}_l = \mathbf{H}_l = \mathbf{I}$, where $\mathbf{I}$ is the identity matrix, based on the assumption that the spectral coherence is constant from segment to segment. This random walk model with process noise provides the flexibility to deal with a range of correlation scenarios, including constant, and slowly and rapidly changing correlation from segment to segment. We assume the noise processes are zero mean, and that the process and observation noise covariance matrices can be represented as $\mathbf{Q}_l = q_l \mathbf{I}$ and $\mathbf{R}_l = r_l \mathbf{I}$, respectively.

These assumptions mean that the state and observation equations, A.1, A.2, process the coherence at each frequency independently and with the same Kalman gain, therefore the Kalman filter gain, $\mathbf{K}_l$, and error $\mathbf{P}_l$ are constant across all frequencies and can be reduced to scalar quantities, denoted K_l and P_l, respectively.

The addition of process noise, $\mathbf{w}_l$, allows changes in correlation to be detected [25]. This process noise covariance, $\mathbf{Q}_l = q_l \mathbf{I}$ has to be specified at each time step. In the original Optimal Spectral Tracking framework, this was fixed throughout the analysis to provide a trade-off between sensitivity and

variability [9]. In the current adaptive framework the process noise is adjusted as each segment is incorporated allowing the Kalman filter to adapt to unusual data [10], or to apply more smoothing if the data between segments is consistent. The observation noise covariance, $\mathbf{R}_l = r_l\mathbf{I}$, is determined from the uncertainty (variance) of the single segment estimator, equation 4. Calculation of r_l is described in section 2.3.

With the above assumptions, the estimate and error for segment l, are given by [9]

$$\mathbf{x}_l = \mathbf{x}_l^p + K_l(\mathbf{z}_l - \mathbf{x}_l^p) \tag{A.3}$$

$$P_l = (1 - K_l)P_l^p. \tag{A.4}$$

Here $\mathbf{x}_l^p$ is the vector of predicted or *a-priori* values and P_l^p is the *a-priori* error. The Kalman filter gain is $K_l = P_l^p(P_l^p + r_l)^{-1}$. In our formulation the predicted error, P_l^p, and corrected error, P_l, apply to all values in $\mathbf{x}_l^p$ and $\mathbf{x}_l$, respectively. The prediction steps are

$$\mathbf{x}_{l+1}^p = \mathbf{x}_l \tag{A.5}$$

$$P_{l+1}^p = P_l + q_l \tag{A.6}$$

where q_l is the variance of the process noise for segment l. The filter is initialised as $\mathbf{x}_1 = \mathbf{z}_1$, $P_1 = r_1$. The tracking process proceeds recursively from $l = 2, \ldots, L$ using equations A.3, A.4.

Kalman smoothing is incorporated using the approach in [9, 42]. This implements a backward smoothing pass over the segments, starting from the final segment. Using $\tilde{\mathbf{x}}_l$ and $\tilde{P}_l$ to represent the vector of smoothed z-transformed coherency values and error, respectively, for segment l the backward smoothing is implemented as

$$\tilde{\mathbf{x}}_l = \mathbf{x}_l + A_l(\tilde{\mathbf{x}}_{l+1} - \mathbf{x}_{l+1}^p) \tag{A.7}$$

$$\tilde{P}_l = P_l + A_l^2\left(\tilde{P}_{l+1} - P_{l+1}^p\right) \tag{A.8}$$

where A_l is the Kalman gain for the backward pass, $A_l = P_l\left(P_{l+1}^p\right)^{-1}$. The smoothing process proceeds recursively from $l = (L-1), \ldots, 1$ using equations A.7, A.8. The smoothing process is initialised as $\tilde{x}_L = \mathbf{x}_L$, $\tilde{P}_L = P_L$, the final segment is fully conditioned on all available segments after tracking.

Appendix B. Algorithmic description of z-tracker.

This Appendix contains an algorithmic level description of the z-tracker, with reference to the relevant equations or sections.

Algorithm 1 z-tracker

Input: x, y, L, T, α
Output: $|\hat{R}_{yx}(\lambda_j, l)|^2$

Initialize: Calculate $\hat{z}_1, r_1$. $P_1 = r_1, K_1 = 1, q_1 = 0$
for $l = 2$ **to** L **calculate:**
  $\hat{z}_l$, equation (4)
  r_l, section (2.3)
  x_l^p, equation (A.5)
  q_l', equation (6)
  q_l, equation (7)
  P_l^p, equation (A.6)
  K_l, x_l, P_l, equations (A.3, A.4)
end for
Initialize reverse pass: $\tilde{x}_L = x_l, \tilde{p}_L = p_l$
for $l = L - 1$ **to** 1 **calculate:**
  $A_l, \tilde{x}_l, \tilde{P}_l$, equations (A.7, A.8)
end for
Bias correction, map to coherence: equation(8)

References

[1] Addison PS (2002) The Illustrated Wavelet Transform Handbook. Institute of Physics, Bristol.

[2] Baraniuk RG, Bayram M (2000) Multiple Window Time Varying Spectrum Estimation. In: Nonlinear and Nonstationary Signal Processing, eds Fitzgerald WJ, Smith RL, Walden AT, Young P. Cambridge University Press, Cambrige. pp 292 - 313.

[3] Ba D, Babadi B, Purdon PL, Brown EN (2014). Robust spectrotemporal decomposition by iteratively reweighted least squares. Proceedings of the National Academy of Sciences, 111(50), E5336-E5345.

[4] Bloomfield P (2002) Fourier analyis of time series - An introduction, 2nd ed. John Wiley & Sons Inc. New York.

[5] Bokil H, Purpura K, Schoffelen J-M, Thomson D, Mitra P (2007). Comparing spectra and coherences for groups of unequal size. Journal of Neuroscience Methods, 159: 337-345.

[6] Brillinger DR (1974) Fourier analysis of stationary processes. Proceedings of the IEEE, 62: 1628-1643.

[7] Brillinger DR (1975) Time Series - Data Analysis and Theory. Holt Rinehart & Winston Inc. New York.

[8] Brittain J-S, Halliday DM, Conway BA, Nielsen JB (2007) Single-trial multiwavelet coherence in application to neurophysiological time series. IEEE Transactions on Bio-Medical Engineering, 54(5), 854-62.

[9] Brittain J-S, Catton C, Conway BA, Nielsen JB, Jenkinson N, Halliday, DM (2009) Optimal spectral tracking-with application to speed dependent neural modulation of tibialis anterior during human treadmill walking. Journal of Neuroscience Methods, 177(2), 334-347.

[10] Brittain J-S, Halliday DM (2011) Optimal spectral tracking-Adapting to dynamic regime change. Journal of Neuroscience Methods, 195(1), 111-115.

[11] Brown RG, Hwang PYC (1997) Introduction to Random Signals and Applied Kalman Filtering, 3rd ed. John Wiley & Sons, New York.

[12] Bruns A (2004) Fourier-, Hilbert- and wavelet-based signal analysis: are they really different approaches? Journal of Neuroscience Methods, 137(2), 321-332.

[13] Carter GC (1987) Coherence and time delay estimation. Proceedings of the IEEE, 75(2), 236-255.

[14] Carter GC, Knapp C, Nuttall A (1973) Statistics of the estimate of the magnitute-coherence function. IEEE Transactions on Audio and Electroacoustics, 21(4), 388-389.

[15] Carter GC, Knapp C, Nuttall A (1973) Estimation of the

magnitude-squared coherence function via overlapped fast Fourier transform processing. IEEE Transactions on Audio and Electroacoustics, 21(4), 337-344.

[16] Chronux.org (2017). [online] Available at: http://chronux.org/ [Accessed 19 Dec. 2017].

[17] Cohen EAK, Walden AT (2010) A Statistical Analysis of Morse Wavelet Coherence. IEEE Transactions on Signal Processing, 58(3), 980-989.

[18] Cohen EAK, Walden AT (2010) A Statistical Study of Temporally Smoothed Wavelet Coherence. IEEE Transactions on Signal Processing, 58(6), 2964-2973.

[19] Cohen EAK, Walden AT (2011) Wavelet Coherence for Certain Nonstationary Bivariate Processes. IEEE Transactions on Signal Processing, 59(6), 2522-2531.

[20] Cohen L (1995) Time-Frequency Analysis. Prentice-Hall Inc. New Jersey.

[21] Enochson LD, Goodman NR (1965). Gaussian approximations to the distribution of sample coherence. Technical Report, AD0620987, Measurement Analysis Corp, Los Angelas. Available from `http://oai.dtic.mil/oai/oai?verb=getRecord&metadataPrefix=html&identifier=AD0620987`

[22] Frigo M, Johnson SG (2005) The Design and Implementation of FFTW3. Proceedings of the IEEE, 93(2), 216-231.

[23] Gabor, D (1946) Theory of communication. Part 1: The analysis of information. Journal of the Institution of Radio and Communication Engineering, 93(26), 429-441.

[24] Halliday DM, Rosenberg JR, Amjad AM, Breeze P, Conway BA, Farmer SF (1995) A framework for the analysis of mixed time series/point process data - Theory and application to the study of physiological tremor, single motor unit discharges and electromyograms. Progress in Biophysics and molecular Biology, 64: 237-278.

[25] Jazwinski AH (1969) Adaptive filtering. Automatica, 5(4), 475-485.

[26] Jazwinski AH (1970) Stochastic Processes and Filtering Theory. Academic Press, New York.

[27] Kalman RE (1960) A New Approach to Linear Filtering and Prediction Problems. Transactions of the ASME-Journal of Basic Engineering, 82, Series D, 35-45.

[28] Lilly JM Olhede SC (2009) Higher-Order Properties of Analytic Wavelets. IEEE Transactions on Signal Processing, 57(1), 146-160.

[29] Lilly JM Olhede SC (2010) On the Analytic Wavelet Transform. IEEE Transactions on Information Theory, 56(8), 4135-4156.

[30] Lilly JM Olhede SC (2012) Generalized Morse Wavelets as a Superfamily of Analytic Wavelets. IEEE Transactions on Signal Processing, 60(11), 6036-6041.

[31] MATLAB Release 2016a, The MathWorks, Inc., Natick, Massachusetts, United States.

[32] McGill R Tukey JW Larsen WA. (1978) Variations of Box Plots. The American Statistician, 32(1), 12-16.

[33] Milde T Leistritz L Astolfi L Miltner WHR Weiss T Babiloni F Witte H (2010) A new Kalman filter approach for the estimation of high-dimensional time-variant multivariate AR models and its application in analysis of laser-evoked brain potentials. NeuroImage, 50(3), 960-969.

[34] Möller E Schack B Arnold M Witte H (2001) Instantaneous multivariate EEG coherence analysis by means of adaptive high-dimensional autoregressive models. Journal of Neuroscience Methods, 105(2), 143-158

[35] Nielsen JB, Conway BA, Halliday DM, Perreault M-C, Hultborn H (2005) Organization of common synaptic drive to motoneurones during fictive locomotion in the spinal cat. Journal of Physiology, 569, 291-304.

[36] Olhede SC, Walden AT (2002) Generalized Morse wavelets. IEEE Transactions on Signal Processing, 50: 2661-2670.

[37] Ostwald D, Kirilina E, Starke L, Blankenburg F (2014) A tutorial on variational Bayes for latent linear stochastic time-series models. Journal of Mathematical Psychology, 60, 1-19.

[38] Percival DB, Walden AT (1993) Spectral Analysis for Physical Applications. Cambridge Univ. Press, UK.

[39] Priestley MB (1981) Spectral analysis and time series. Academic Press, London.

[40] Priestley MB (1988) Non-linear and Non-stationary Time Series Analysis. Academic Press, London.

[41] Priestley MB (1996) Wavelets and Time-dependent Spectral Analysis. Journal of Time Series Analysis, 17(1), 85-103.

[42] Rauch HE, Tung F, Striebel CT (1965) Maximum likelihood estimates of linear dynamic systems. AIAA Journal, 3(8), 1445-1450.

[43] Rosenberg JR, Amjad A, Breeze P, Brillinger DR, Halliday DM (1989). The Fourier approach to the identification of functional coupling between neuronal spike trains. Progress in Biophysics and Molecular Biology, 53: 1-31.

[44] Siegel M, Donner TH, Engel AK (2012) Spectral fingerprints of large-scale neuronal interactions. Nature Reviews Neuroscience, 13(2), 121-134.

[45] Stevenson CW, Halliday DM, Marsden CA, Mason R (2007) Systemic administration of the benzodiazepine receptor partial inverse agonist FG-7142 disrupts corticolimbic network interactions. Synapse, 61(8), 646-663.

[46] Thomson DJ (1982) Spectrum estimation and harmonic analysis. Proceedings of the IEEE, 70: 1055-1096.

[47] Thomson DJ, Chave A (1991) Jackknifed error estimates for spectra, coherences, and transfer functions. In S. Haykin (Ed.), Advances in spectrum analysis and array processing, 1. pp 58-113.

[48] Torrence C, Compo G (1998) A practical guide to wavelet analysis. Bulletin of the American Meteorological Society, 79(1), 61-78.

[49] Walden AT, Cohen EAK (2012) Statistical Properties for Coherence Estimators From Evolutionary Spectra. IEEE Transactions on Signal Processing, 60(9), 4586-4597.

[50] Welch P (1967) The use of fast Fourier transform for the estimation of power spectra: a method based on time averaging over short, modified periodograms. IEEE Transactions on Audio and Electroacoustics, 15(2), 70-73.

[51] Xu Y, Haykin S, Racine RJ (1999) Multiple window time-frequency distribution and coherence of EEG using Slepian sequences and Hermite functions. IEEE Transactions on Biomedical Engineering, 46(7), 861-866.

[52] Zhan Y, Halliday DM, Jiang P, Liu X, Feng J (2006) Detecting time-dependent coherence between non-stationary electrophysiological signals–a combined statistical and time-frequency approach. Journal of Neuroscience Methods, 156(1-2), 322-332.